

Rapid electrophoretic deposition of biocompatible graphene coatings for high-performance recording neural electrodes

Miheng Dong^{a, d}, Harold A. Coleman^b, Mary A. Tonta^b, Zhiyuan Xiong^c, Dan Li^c, Sebastian Thomas^a, Minsu Liu^{a, d, e}, James B. Fallon^{f, g}, Helena C. Parkington^{b*}, John S. Forsythe^{a*}*

^a Department of Materials Science and Engineering, Monash Institute of Medical Engineering, Monash University, Clayton, VIC 3800, Australia

^b Department of Physiology, Biomedicine Discovery Institute, Monash University, Clayton, VIC 3800, Australia

^c Department of Chemical Engineering, University of Melbourne, Parkville, Victoria, Australia

^d Monash Suzhou Research Institute, Monash University, Suzhou SIP 250000, China

^e Foshan (Southern China) Institute for New Materials, Foshan 528200, China

^f The Bionics Institute, East Melbourne, Victoria 3002, Australia

^g Medical Bionics Department, University of Melbourne, Parkville, Victoria 3010, Australia

* Co-corresponding authors

S1. Properties of GO flakes in IPA/water dispersion

The average GO flake size used in this study was $6.2 \pm 0.2 \mu\text{m}$ ($N = 209$) (Figure S1, S2a). A small flake size enables deposition onto miniaturized metal electrodes. The thickness of single-layer GO was 1.1 nm (Figure S1, inset), comparable to previous reports,¹⁻³ indicating effective oxidation and exfoliation of GO. Zeta potentials (ZP) of GO particles (1.5 mg ml^{-1}) in IPA90/water10 mixture were $-44.0 \pm 1.9 \text{ mV}$, which is significantly lower than -30 mV (Figure S2b), the threshold value of moderate colloidal stability.^{4, 5} This explains the stability of GO dispersion over a long period (typically a few months) and the deposition of GO flakes onto the positively charged electrode during the electrophoretic deposition (EPD). ZP were measured for a wide range of GO concentrations (0.05 mg ml^{-1} GO: ZP = $-44.0 \pm 1.7 \text{ mV}$; 0.1 mg ml^{-1} GO: ZP = $-45.3 \pm 2.6 \text{ mV}$; 0.5 mg ml^{-1} GO: ZP = $-41.4 \pm 1.7 \text{ mV}$; 1.0 mg ml^{-1} GO: ZP = $-39.2 \pm 1.9 \text{ mV}$). Small variations in ZP exist between different GO concentrations and there is no statistical difference from the 1.5 mg ml^{-1} GO group (Figure S2c). This indicates that the ZPs are not induced by concentration artifacts.⁶

S2. Comparison of GO/IPA/water against GO/NaCl/water dispersion

Due to the voltage limited by water electrolysis, conventional GO (1.5 mg ml^{-1}) EPD conducted in aqueous NaCl dispersion (0.5 M) had a slow deposition rate and gas bubbles from water electrolysis impeded the formation of a complete coating.⁷⁻⁹ At -1.1 V , the generation of gas was observed under the microscope (Movie S2). Since gas bubbles impede the deposition of GO flakes on the electrode, the voltage was increased to -1.0 V and no gas generation was observed (Movie S3). At this potential, the deposition of GO in NaCl dispersion is slower than the use of GO in IPA. After deposition of 1 hour, only a trivial amount of GO was successfully deposited onto the electrode. To reduce the generation of gas and yield a faster deposition process, GO was dispersed in IPA/water. Therefore, it is possible to increase the bias voltage

to + 10 V, about one order of magnitude greater than that used in the GO/NaCl/water system, significantly reducing the depositing time from 1 hour to a few minutes. Also, compared to CVD, a process which requires a high temperature ($> 1000\text{ }^{\circ}\text{C}$) and low pressure ($< 100\text{ Pa}$),¹⁰ the improved EPD can deposit at a fast rate in mild conditions.^{11, 12} The production is scalable and continuous, with the possibility to control the morphology and thickness of the coatings, making it suitable to precisely deposit GO on exposed electrode tips without damaging the polyphenylsulfone (PPSU) insulation.

S3. XPS of graphite, GO and ErGO

Summarized in Table S1, C=C/C-C, C-OH, C-O-C, C=O, and O-C=O were identified from C1s spectra with peaks centered at 284.1-284.5, 285.5, 286.7-286.9, 288.0-288.3, 289.0 eV, respectively (Figure 1e, f). Fit-peak positions are consistent with previous publications.¹³⁻¹⁵ It is noted that, after the electrochemical reduction, the majority of epoxide groups were reduced to C=C/C-C and the rest formed C-OH bonds (Table S1). The C=O and O-C=C ratios remained almost unchanged during the reduction process. The O-C=O ratio was very small compared with other peaks, indicating that GO and ErGO are prepared to have a low concentration of defects (edges and holes).¹⁶ Some oxygen-containing residuals still exist in ErGO compared with graphite (Figure S7).

S4. Raman spectroscopy of graphite, GO and ErGO

Similar to previous publications,^{17, 18} four bands, at $\sim 1350\text{ cm}^{-1}$ (D), $\sim 1590\text{ cm}^{-1}$ (G), $\sim 2690\text{ cm}^{-1}$ (2D), and 2930 cm^{-1} (D+G), were identified from GO and ErGO samples (Figure 1g). The low D peak intensity in graphite samples suggests that graphite was almost free of defects. The reduction process from GO to ErGO increased $I_{\text{D}}/I_{\text{G}}$ ratio from 1.02 to 1.15. The slight increase was attributed to the decrease in average sp^2 domain size. Similar phenomena were observed

on samples reduced by hydrazine¹⁵ and electrochemical reduction.⁹ The spectrum of GO showed the presence of multiple peaks. An intense band at 3400 cm⁻¹ was associated with the O-H stretching vibrations of hydroxy and/or carboxyl groups in the structure. Weak bands at 2925 cm⁻¹ and 2851 cm⁻¹ were due to the asymmetric and symmetric stretching vibration of C-H bond, respectively. Bands at 1726 cm⁻¹ (carbonyl C=O stretching vibration), 1621 cm⁻¹ (C=C stretching vibration of un-oxidized domains), 1373 cm⁻¹ (O-H deformation), 1228 cm⁻¹ (C-O stretching vibration of epoxy groups), and 1074 cm⁻¹ (C-O stretching of alkoxy groups).¹⁹⁻²¹

S5. XRD of graphite, GO and ErGO

Results of XRD spectra are summarized in Table S2. For pristine graphite powder, the 2 θ peak position was at 26.49° (FWHM = 0.31°), equivalent to an interlayer distance of 3.36 Å. GO showed a 2 θ peak at 10.12° (FWHM = 1.17°), indicating that the graphite powder had been highly oxidized into GO with an interlayer distance of 8.73 Å. In comparison to graphite, exfoliated GO had a smaller average height of stacking layers (H = 7 nm) and a lower average number of layers (n = 8, approx.). The average stacking layer height of ErGO was 1 nm with approximately 3 graphene sheets in each nanostructure. The interlayer thickness of ErGO was 3.62 Å, which was slightly larger than pristine graphite due to some residual oxygen functional groups remaining on ErGO. Similar results were found in the reduction of GO using aluminum powder,²² hydrazine,^{23, 24} hydroiodic acid,²⁵ amino acid,² and microwave (mild thermal reduction).²⁶

S6. Optimization of selective coating parameters with FEM.

The EPD of GO was conducted in a 3D space. Given that the array extended along the z-axis, it was reasonable to simplify the simulation to the x-O-y plane. GO was characterized as negatively charged and thus it would migrate/move in the counter direction to the electric field. When +10V was applied to the working electrode (E2), it emitted the electric field from E2 to the GO dispersion (Figure S19a). All GO particles moved towards E2. Since the movement of GO flakes along x-axis (horizontal movement) did not influence whether the GO would deposit on the array, the total electric field was further split into vectors along the x and y axes, and only the y direction was investigated. The original setup (setup 0) with +10 V on working electrodes resulted in a positive y-directional electric field in the whole space of GO dispersion (Figure S20a), meaning that all GO flakes in the dispersion would move toward the surface of electrode array. Changing the adjacent electrodes to negative bias -10 V (setup 1) meant current would move to E1 and E3 (Figure S19b), forming a negative y-directional electric field near the adjacent electrodes (Figure S20b) to direct the GO in this area away from the surface. To enlarge the area with negative y-directional electric field, a +1 V on WE and -15V on adjacent electrodes setup (setup 2) was tested (Figure S19c). In general, the area with positive y split was significantly reduced (Figure S20 b-c). However, for the area immediately above the array, ~50 % of the area still exhibited a positive y-directional electric field, meaning the deposition of GO on the inter-electrode insulation could not be avoided, with a 15 times difference between balancing (applied to the electrodes adjacent to WE) and WE voltage. From previous experience, the voltage on WE was directly related to the speed of GO EPD and a higher voltage on the counter would cause electrolysis of IPA/water. The final setup (setup 3) was decided to be +10 V on WE with -15 V on adjacent electrodes (Figure S19 d). This offered a relatively high coating speed, with similar effectiveness to setup 2 in limiting the deposition of GO (in the area near the array-dispersion interface) onto array (Figure 6c, S20 c).

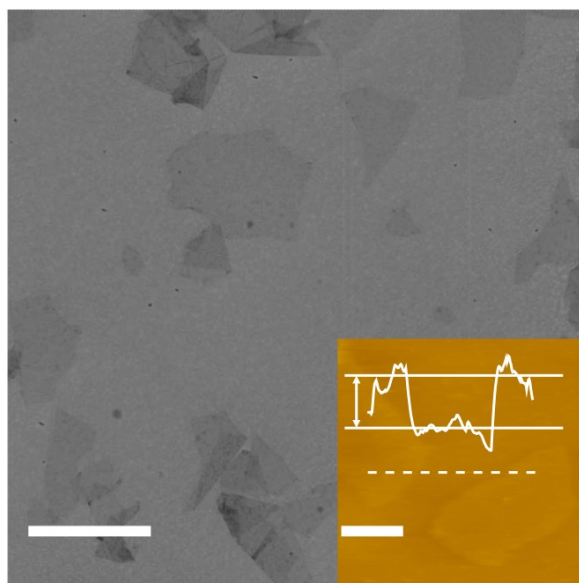


Figure S1. SEM of GO flakes. Inset: AFM image of monolayer graphene oxide. GO thickness is 1.5 nm across the dashed line. Scalebar: 10 μm , inset: 3 μm .

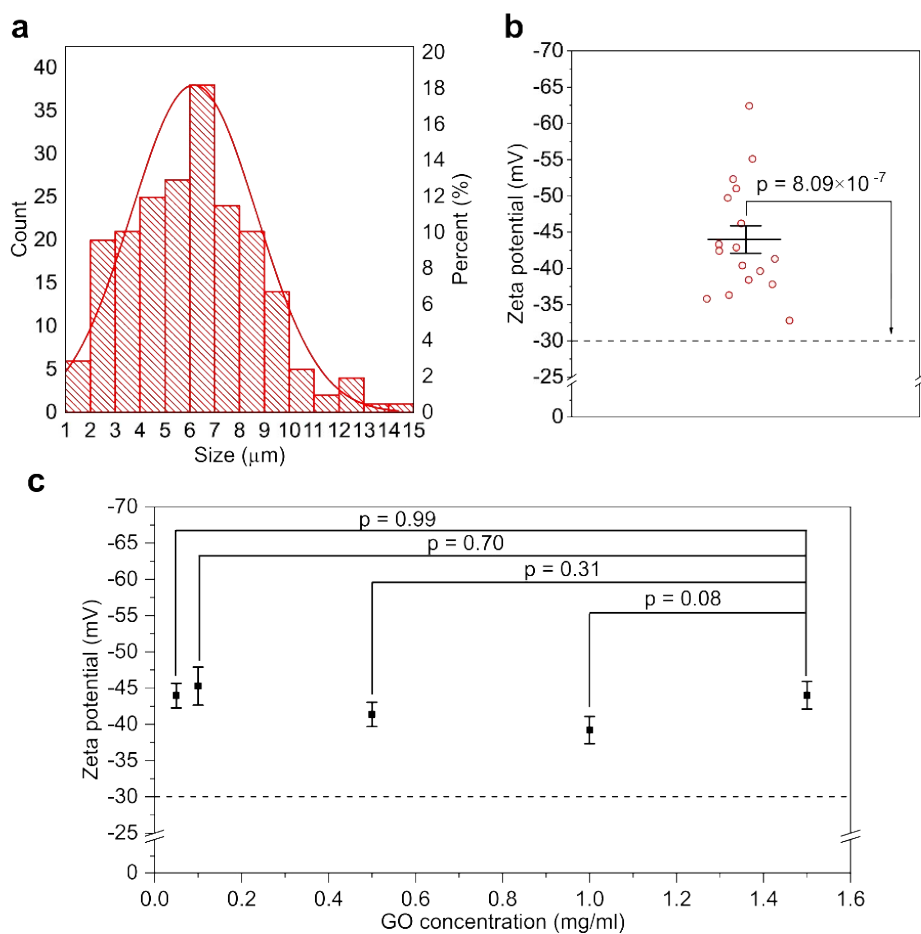


Figure S2. Characterization of GO dispersion. (a) Histogram of GO flake size, fitting curve: normal probability density function. (b) ZP of GO particles in 1.5 mg ml⁻¹ dispersion. (c) ZP of GO particle in IPA90/water 10 (v/v) of various concentrations (0.05, 0.1, 0.5, and 1.0 mg ml⁻¹) in comparison to 1.5 mg ml⁻¹. Error bar: \pm SEM. N numbers for 0.05, 0.1, 0.5, and 1.0 mg ml⁻¹ GO particle concentrations are 19, 17, 18, and 19, respectively. To characterize the colloidal stability of 1.5 mg/ml GO, one-sample t-test was used with the test mean = -30 (mV), $p = 8.09 \times 10^{-7}$ (N = 17). To compare the ZP value between 1.5 mg/ml GO and other concentrations, two-sample t-test was used.

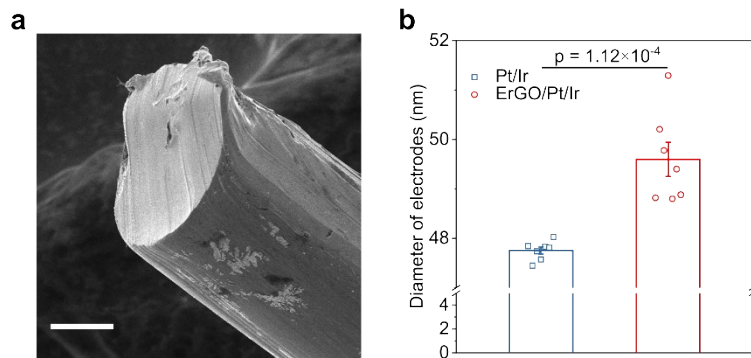


Figure S3. Characterization of ErGO/Pt/Ir wires. SEM images of (a) a pristine smooth Pt/Ir wire. Scale bar: 15 μm. (b) The change of electrode diameters. Error bar: ± SEM. Two-sample t-test. N = 7.

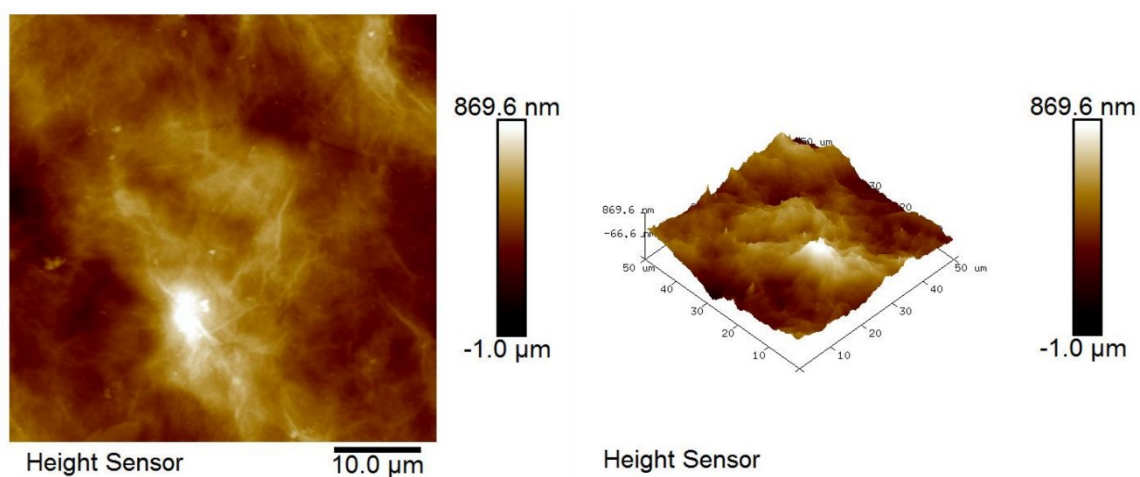


Figure S4. AFM of ErGO on Pt tiles.

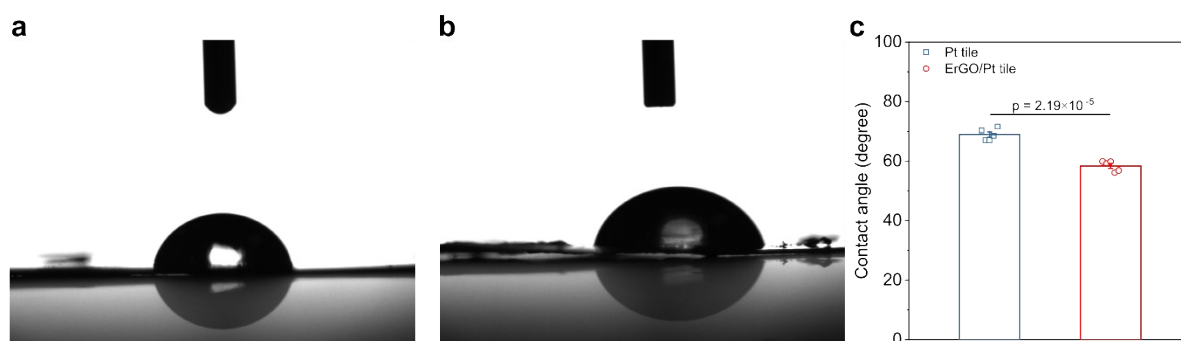


Figure S5. Contact angle of ErGO on Pt tiles. (a) water on Pt tile, (b) water on ErGO/Pt tile, (c) statistical analysis of water angles. Two-sample t-test, $p = 0.0000219$, $N=5$. Error bars: \pm SEM.

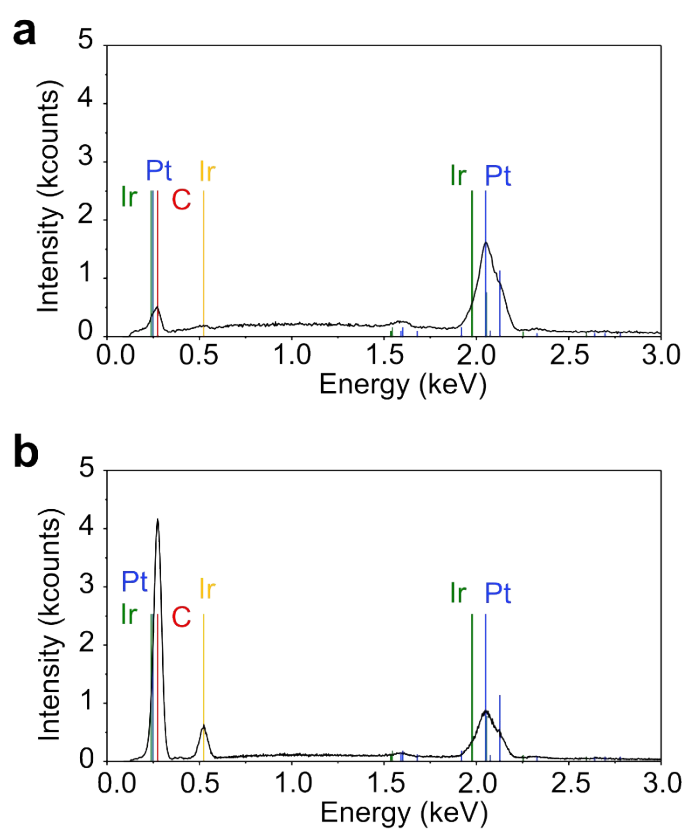


Figure S6. EDX of (a) Pt/Ir and (b) Pt/Ir with thin ErGO coating.

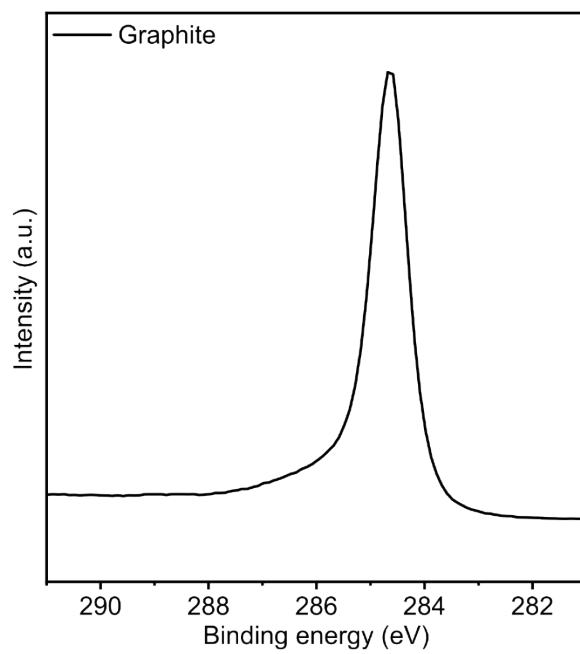


Figure S7. C1s XPS for graphite.

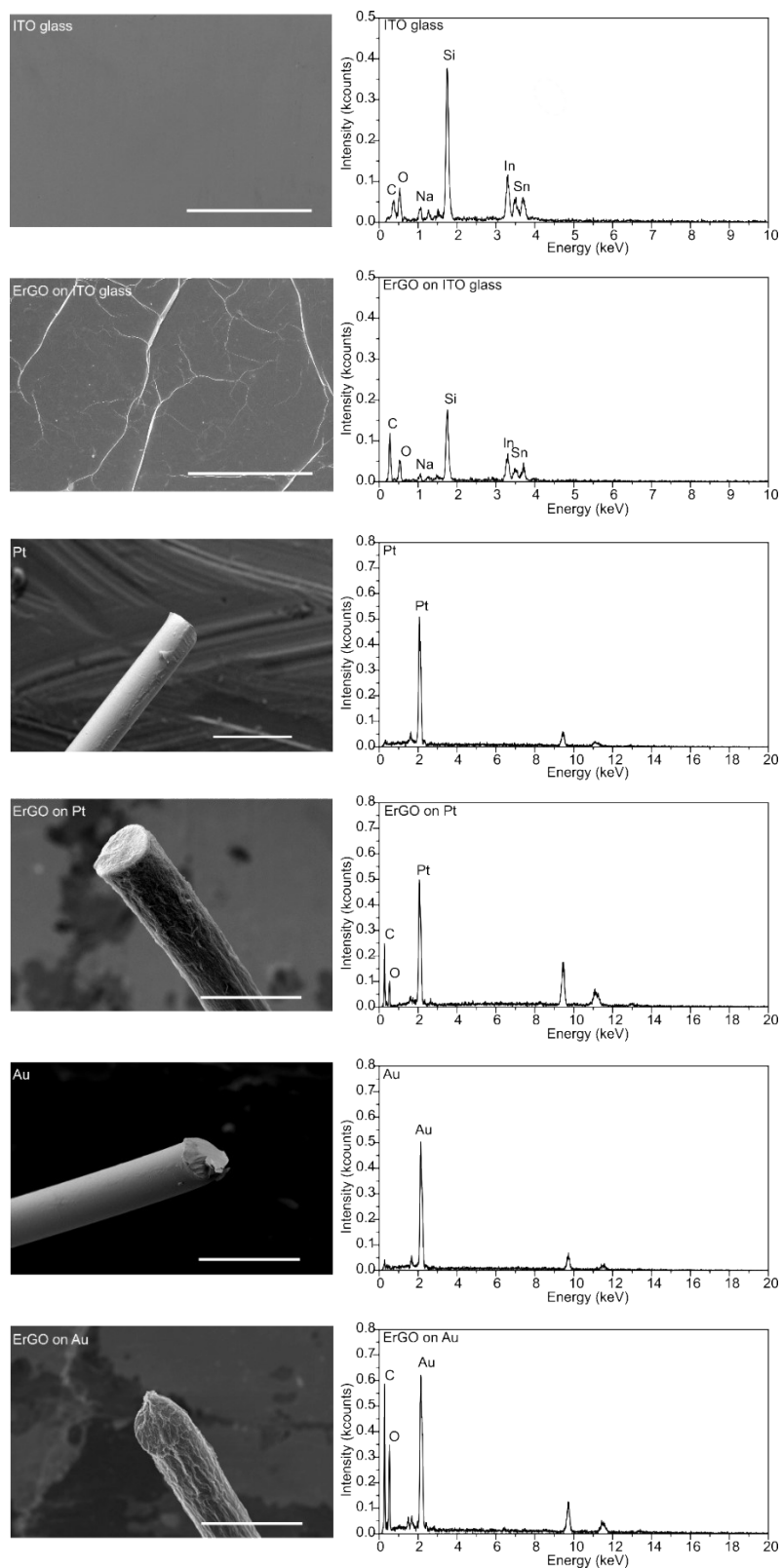


Figure S8. SEM and EDX of ITO glass, ErGO on ITO glass, Pt, ErGO on Pt, Au and ErGO on Au. Scale bars: ITO glass and ErGO on ITO glass: 200 μm ; Pt, ErGO on Pt, Au and ErGO on Au: 100 μm .

Table S1. Fitting result of C1s XPS spectra for GO and ErGO.

	GO			ErGO		
	Binding	Ratio	FWHM	Binding	Ratio	FWHM
	Energy (eV)	(%)	(eV)	Energy (eV)	(%)	(eV)
C=C/C-C	284.53	54.22	1.41	284.13	76.65	1.20
C-OH	285.50	2.98	1.34	285.50	12.82	1.30
C-O-C	286.86	35.32	1.32	286.70	4.58	1.25
C=O	288.25	4.91	1.35	288.02	4.52	1.28
O-C=O	288.98	2.57	1.40	289.00	1.42	1.26

Table S2. Structural parameters of graphite, GO, and ErGO resulting from the XRD patterns.

Notation: H—the average height of stacked layers, d—the average interlayer distance of graphene layers, n—the average number of graphene layers in the stacked structure.

Peak (0 0 2)					
	2 θ (deg)	FWHM (deg)	H (nm)	d (Å)	n
Graphite	26.49	0.31	26	3.36	78
GO	10.12	1.17	7	8.73	8
ErGO	24.54	7.67	1	3.62	3

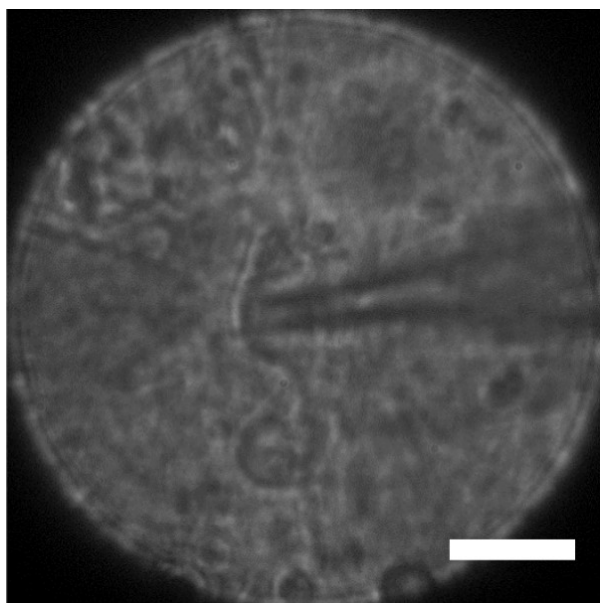


Figure S9. A Patch clamp electrophysiology of rat primary hippocampal neurons cultured on ErGO. A bright field image of a patched cell and the electrode. Scale bar: 20 μm .

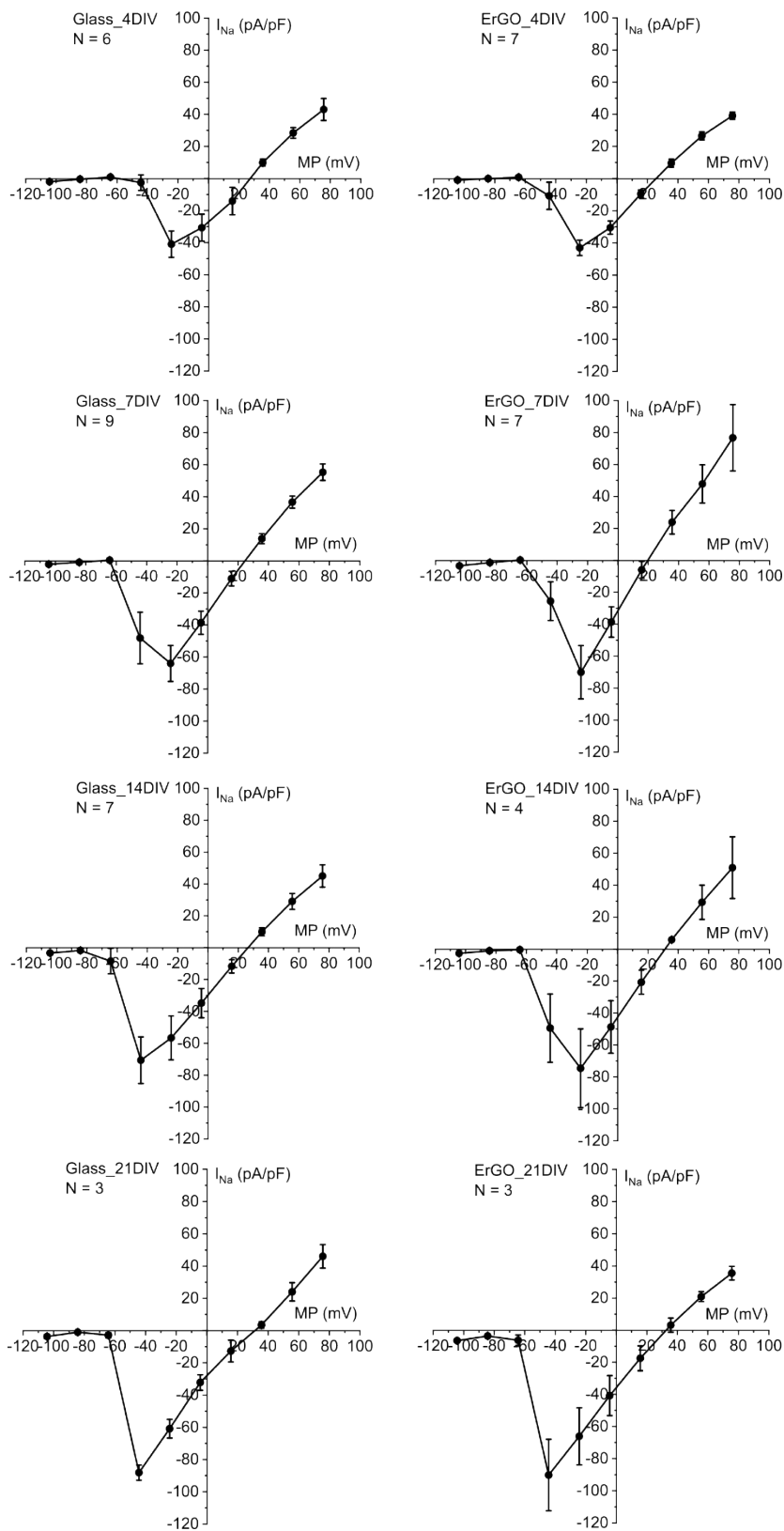


Figure S10. Averaged sodium current–voltage relation for primary neurons sodium channels.

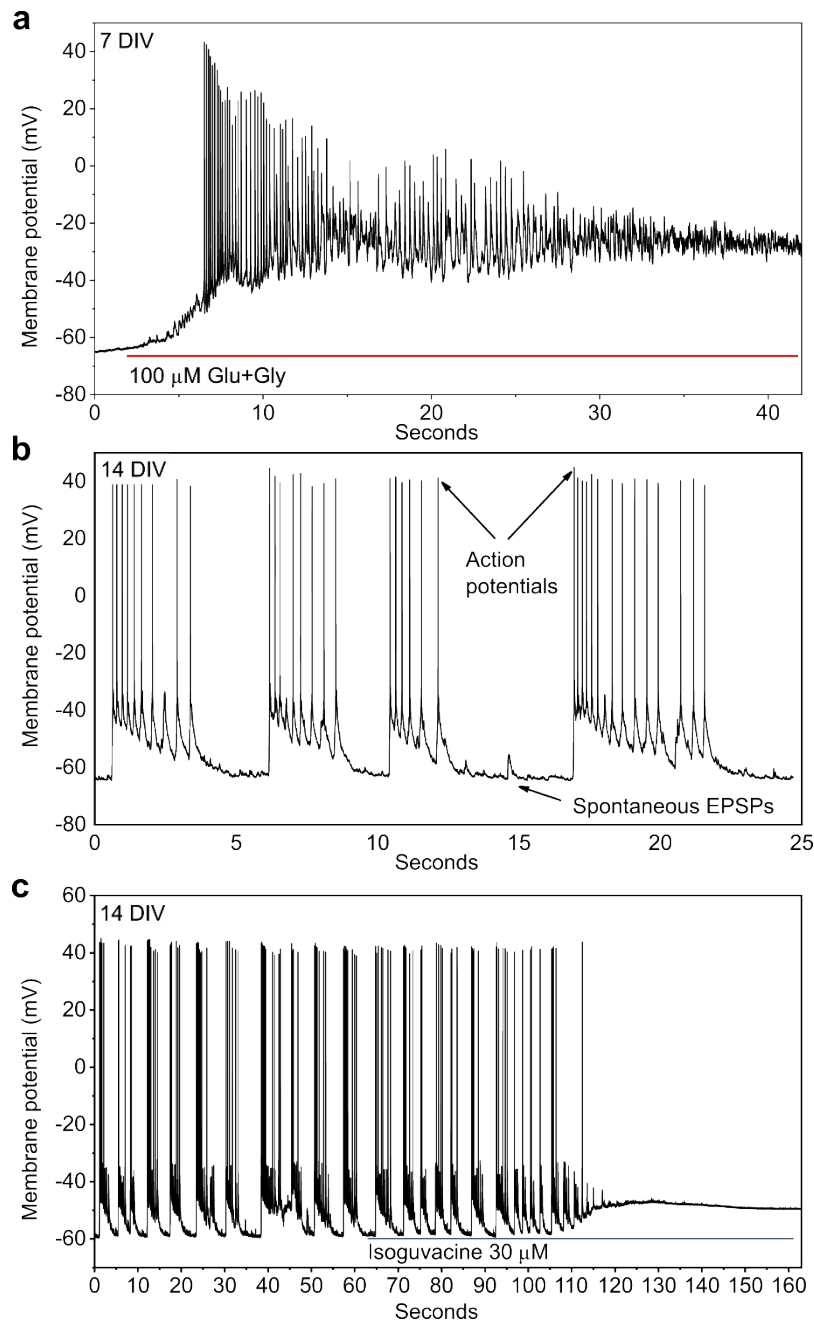


Figure S11. Patch clamp electrophysiology of rat primary hippocampal neurons cultured on glass control. (a) Depolarization of a neuron upon addition of 100 μM glutamate plus glycine (Glu+Gly) on 7 DIV. (b) Organised spontaneous activity of a neuron on 14 DIV. (c) Response to isoguvacine, a GABA_A receptor agonist, on 14 DIV.

Table S3. Probability of two-sample t-test between ErGO and glass control on different DIV across RMP, evoked AP peaks, I_{Na} , and spontaneous AP frequency. N numbers for each group is included in the parentheses after the p value, where G and E stand for glass control and ErGO respectively.

	RMP	Evoked AP peak	I_{Na}	Spont. AP frequency
4 DIV	0.92 (G=7, E=7)	0.98 (G=5, E=5)	0.82 (G=6, E=7)	N/A
7 DIV	0.92 (G=8, E=8)	0.40 (G=6, E=6)	0.76 (G=9, E=7)	0.80 (G=5, E=5)
14 DIV	0.70 (G=8, E=8)	0.67 (G=6, E=6)	0.89 (G=7, E=4)	0.16 (G=5, E=5)
21 DIV	N/A	N/A	0.93 (G=3, E=3)	N/A

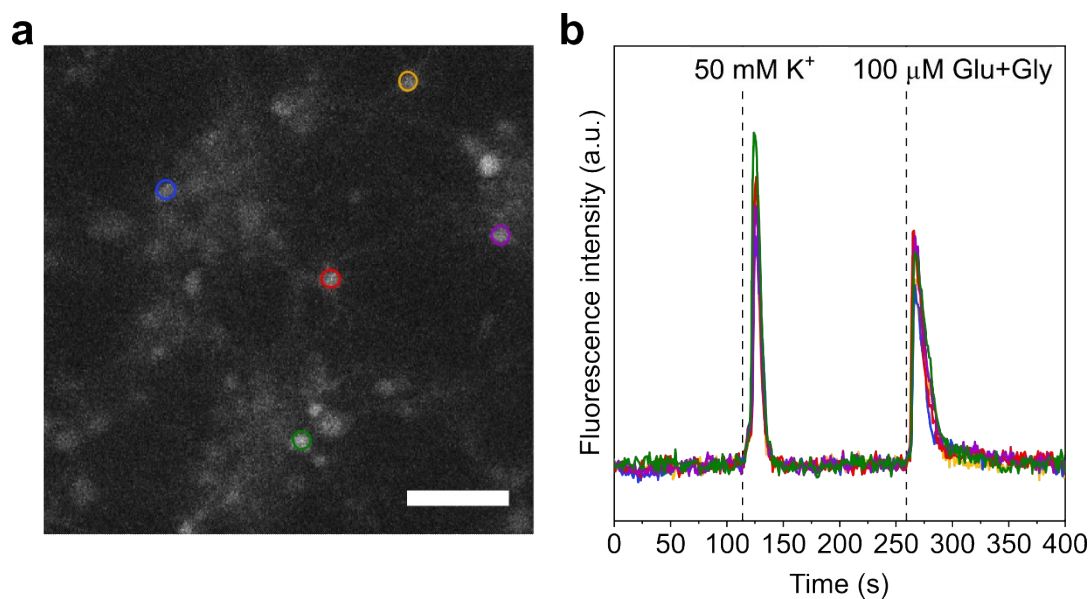


Figure S12. Calcium imaging of primary neurons cultured on glass control (11 DIV). (a) An image of the neurons cultured on glass control with ROIs in circles. (b) Fluorescence intensity of corresponding ROIs. Scale bar: 50 μ m.

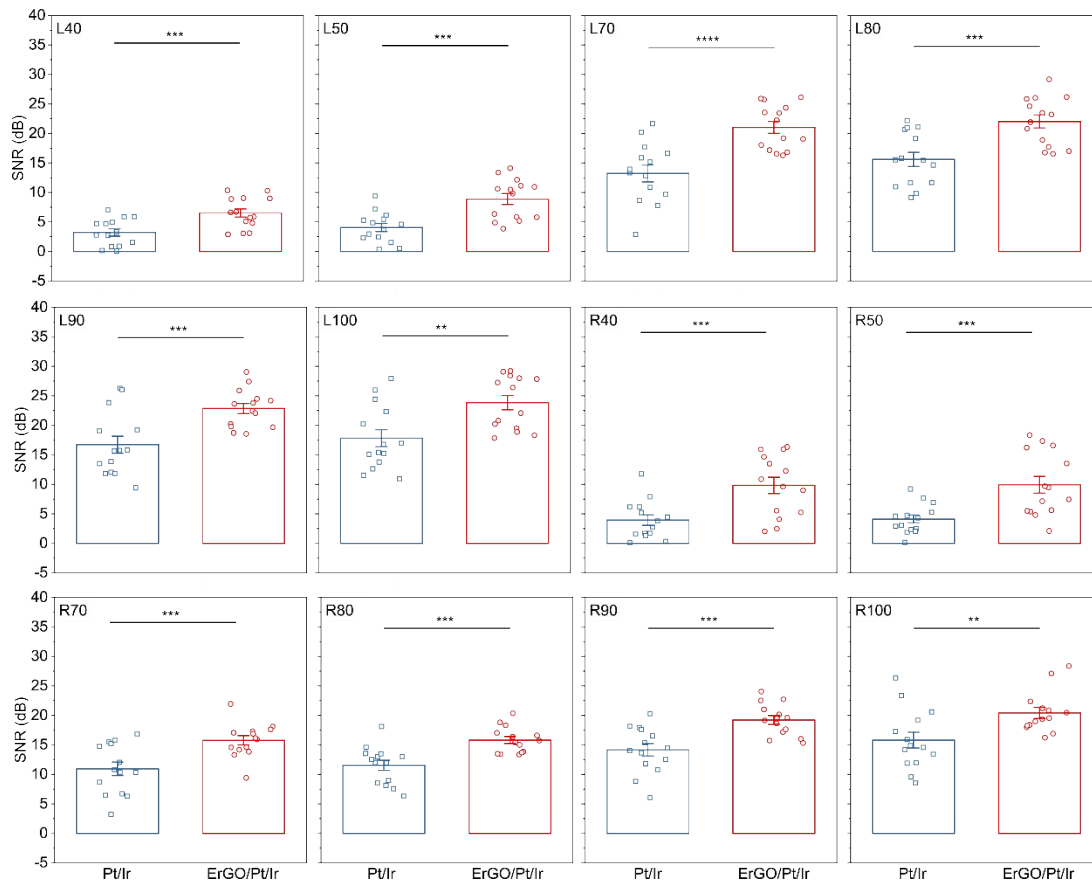


Figure S13. SNRs of acute recordings from cat auditory cortex. SPL at 40, 50, 70, 80, 90, 100 dB. (L) for left auditory cortex and (R) for right auditory cortex.

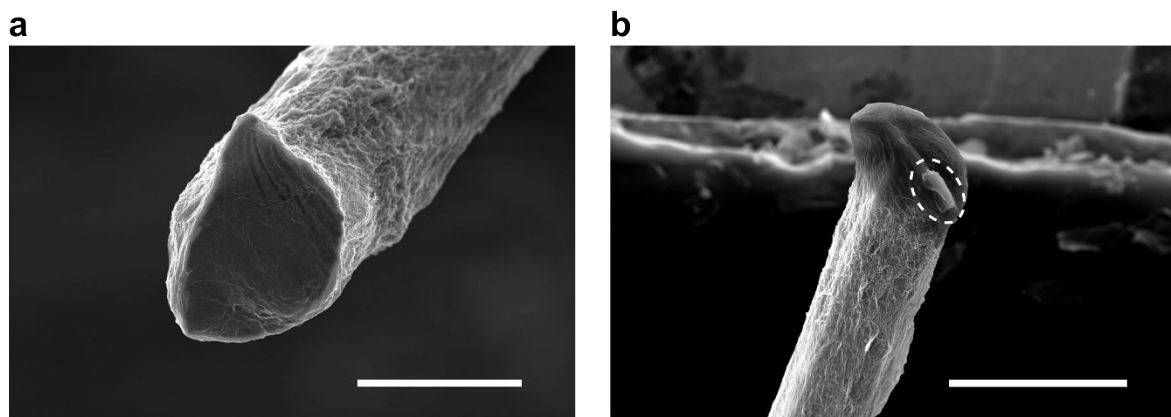


Figure S14. SEM image of ErGO/Pt/Ir electrodes. (a) as prepared, (b) post implantation in 0.6% agarose gel for 48 hr. The residual of gel was circled by the ellipse in dash line. Scale bars: (a) 50 μm , (b) 100 μm .

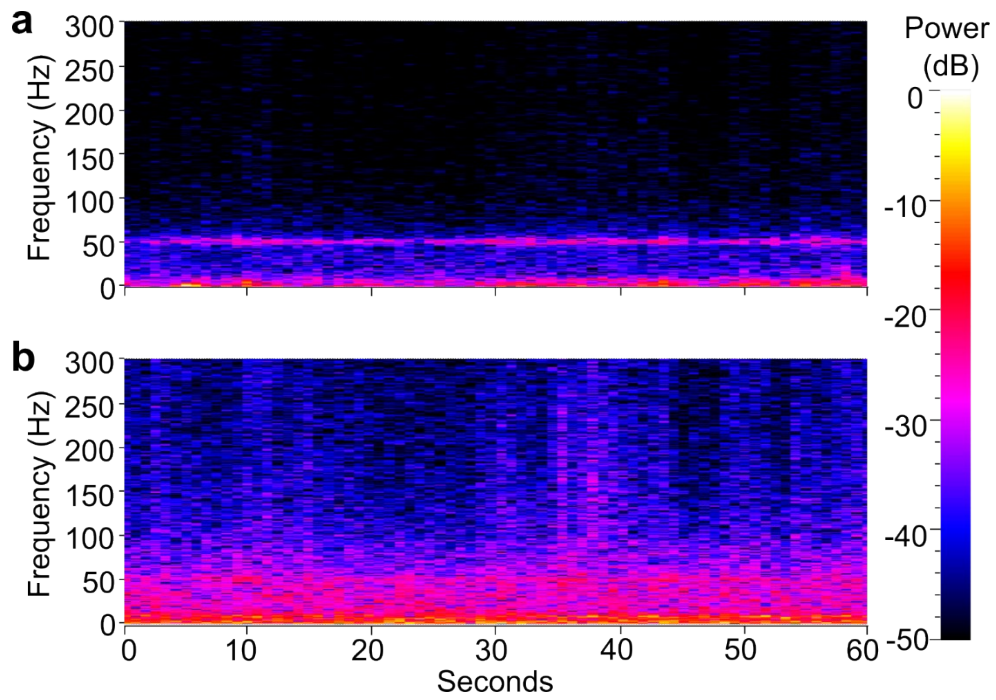


Figure S15. LFPs from rat somatosensory cortex on day 17, over 60 seconds. The power of recordings (1-300 Hz) over time from (a) Pt/Ir and (b) ErGO/Pt/Ir.

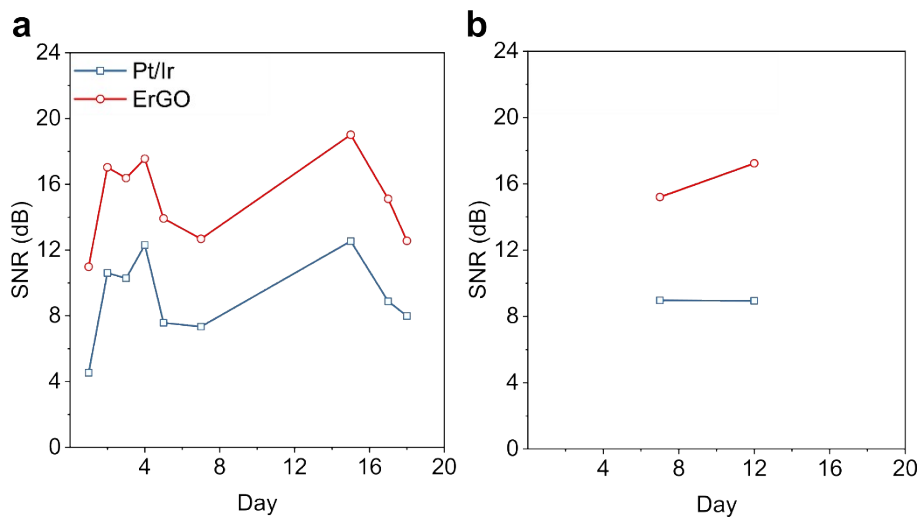


Figure S16. Recordings from rat somatosensory cortex. SNR of multiunit spikes from (a) rat 2, (b) rat 3.

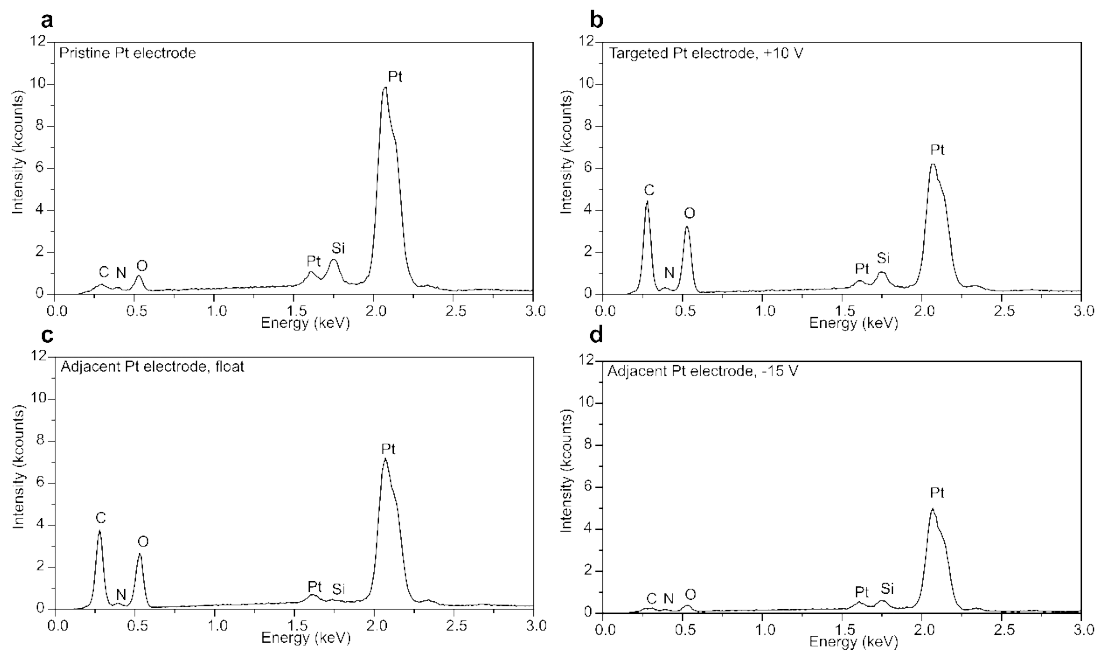


Figure S17. EDX pelvic nerve arrays. (a) pristine Pt electrode; when +10V was applied, EDX from the targeted electrode (b) and the adjacent electrode (c); when both +10 V bias voltage and -15V counter voltage were applied, EDX from the adjacent electrode (d). Silicon peaks were attributed to the use the silicone elastomer during the preparation of nerve arrays.

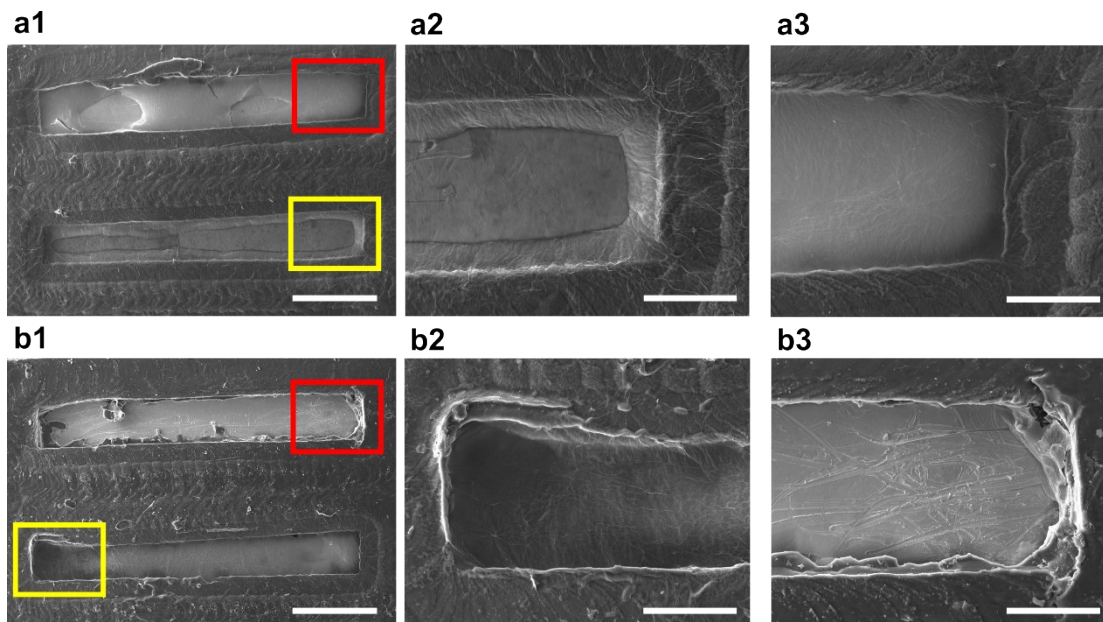


Figure S18. SEM of pelvic array. After +10 V only coating (a1), both the working electrode (a2) and the adjacent electrode (a3) were coated with GO. When +10 V and -15 V were applied

(b1), only the working electrode was coated with GO (b2), the adjacent electrode was free of GO flakes (b3). Yellow and red boxes label the zoom in of working and adjacent electrodes, respectively. Wrinkles on the surface of Pt and silicone elastomer were GO flakes. Scale bars: (a1 & b1) 500 μm , (a2-a3, b2-b3) 150 μm .

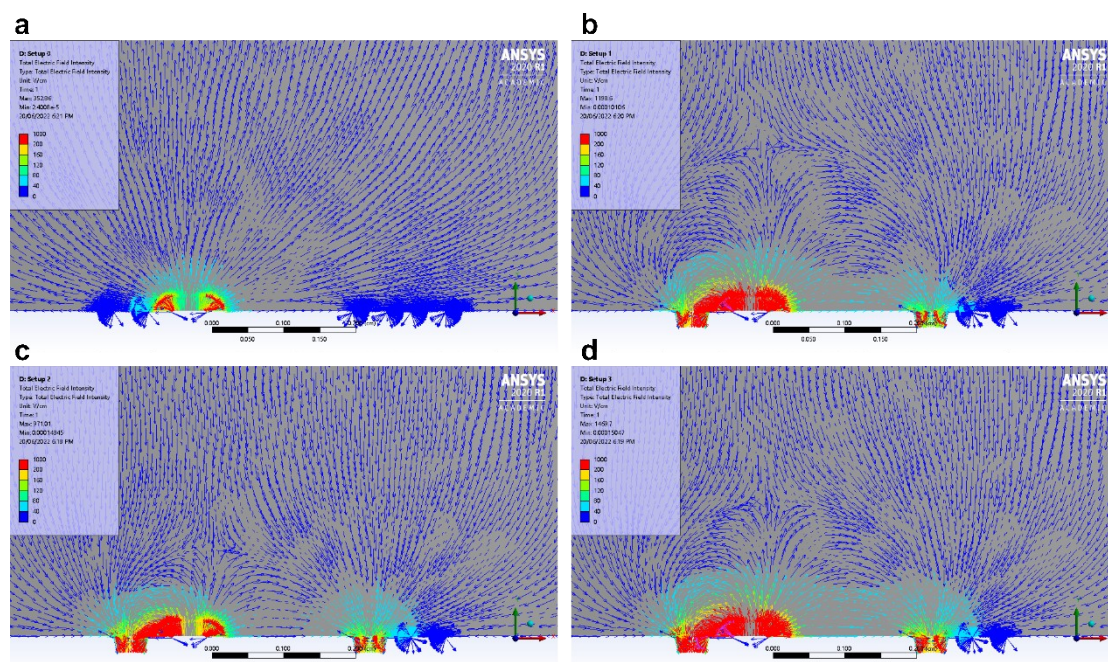


Figure S19. Simulation of electric field in x-O-y plane. (a) Original setup (setup 0), only +10 V was applied to working electrode; (b) +10 V on working electrode, -10 V on adjacent electrodes (setup 1); (c) +1 V on working electrode, -15 V on adjacent electrodes (setup 2); (d) +10 V on working electrode, -15 V on adjacent electrodes (setup 3).

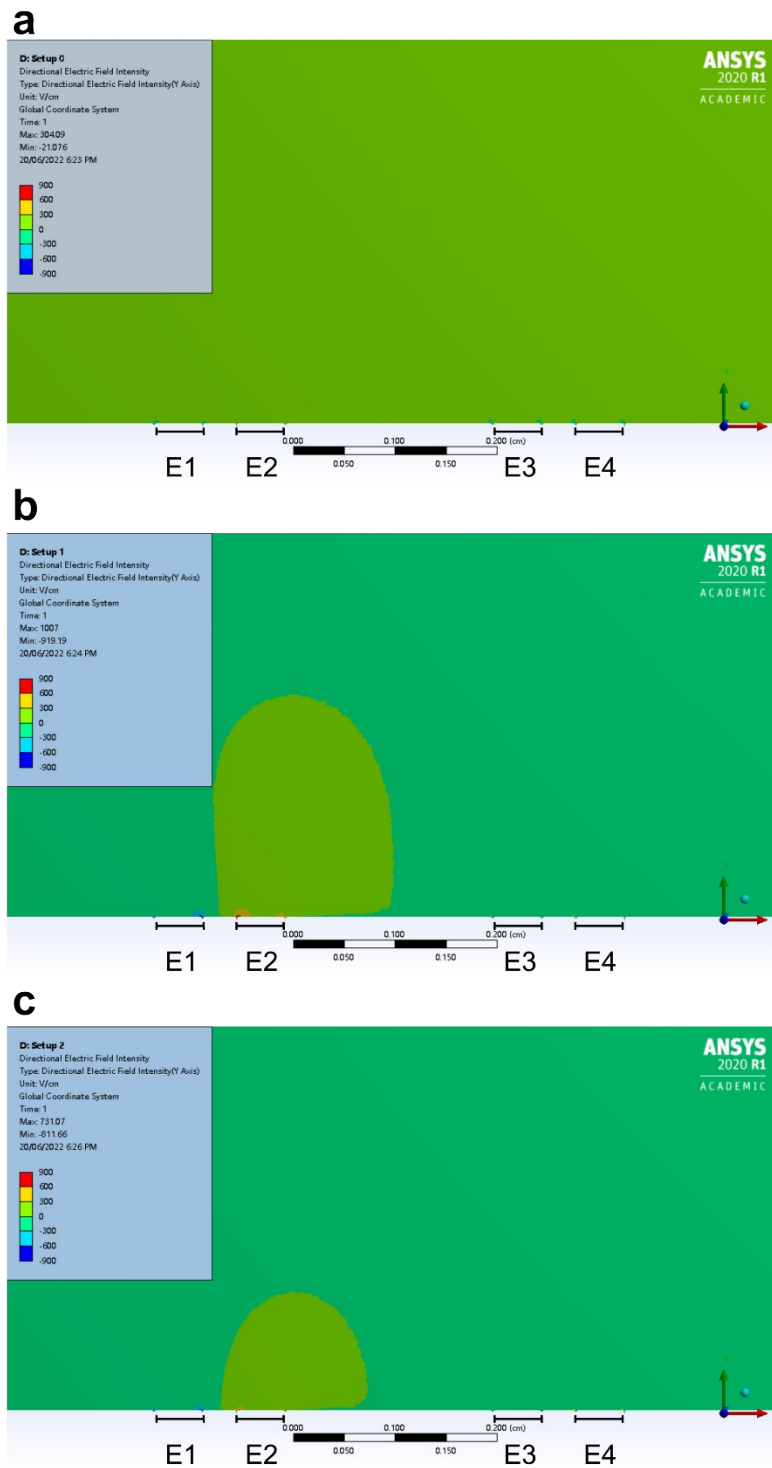


Figure S20. Simulation of y-directional electric field in x-O-y plane. (a) Original setup (setup 0), only +10 V was applied to working electrode; (b) +10 V on working electrode, -10 V on adjacent electrodes (setup 1); (c) +1 V on working electrode, -15 V on adjacent electrodes (setup 2).

References

1. J. Zhang, H. Yang, G. Shen, P. Cheng, J. Zhang and S. Guo, *Chem Commun (Camb)*, 2010, **46**, 1112-1114.
2. D. Chen, L. Li and L. Guo, *Nanotechnology*, 2011, **22**, 325601.
3. S. Yang, W. Yue, D. Huang, C. Chen, H. Lin and X. Yang, *RSC Advances*, 2012, **2**, 8827-8832.
4. D. Parviz, F. Irin, S. A. Shah, S. Das, C. B. Sweeney and M. J. Green, *Adv Mater*, 2016, **28**, 8796-8818.
5. S. Navalon, A. Dhakshinamoorthy, M. Alvaro and H. Garcia, *Chem Rev*, 2014, **114**, 6179-6212.
6. R. Tantra, P. Schulze and P. Quincey, *Particuology*, 2010, **8**, 279-285.
7. A. N. Dalrymple, M. Huynh, U. A. Robles, J. B. Marroquin, C. D. Lee, A. Petrossians, J. J. Whalen, D. Li, H. C. Parkington, J. S. Forsythe, R. A. Green, L. A. Poole-Warren, R. K. Shepherd and J. B. Fallon, *J Neural Eng*, 2019, **17**, 016015.
8. J. A. Bennett, I. B. Agbere and M. Moesta, *Electrochimica Acta*, 2016, **188**, 111-119.
9. M. Hilder, B. Winther-Jensen, D. Li, M. Forsyth and D. R. MacFarlane, *Phys Chem Chem Phys*, 2011, **13**, 9187-9193.
10. S. Zhao, X. Liu, Z. Xu, H. Ren, B. Deng, M. Tang, L. Lu, X. Fu, H. Peng, Z. Liu and X. Duan, *Nano Letters*, 2016, **16**, 7731-7738.
11. M. Diba, D. W. H. Fam, A. R. Boccaccini and M. S. P. Shaffer, *Progress in Materials Science*, 2016, **82**, 83-117.
12. A. R. Boccaccini, J. Cho, J. A. Roether, B. J. C. Thomas, E. Jane Minay and M. S. P. Shaffer, *Carbon*, 2006, **44**, 3149-3160.
13. R. Wang, Y. Wang, C. Xu, J. Sun and L. Gao, *RSC Adv.*, 2013, **3**, 1194-1200.

14. X. Z. Tang, Z. Cao, H. B. Zhang, J. Liu and Z. Z. Yu, *Chem Commun (Camb)*, 2011, **47**, 3084-3086.
15. D. Yang, A. Velamakanni, G. Bozoklu, S. Park, M. Stoller, R. D. Piner, S. Stankovich, I. Jung, D. A. Field, C. A. Ventrice and R. S. Ruoff, *Carbon*, 2009, **47**, 145-152.
16. S. Kim, S. Zhou, Y. Hu, M. Acik, Y. J. Chabal, C. Berger, W. de Heer, A. Bongiorno and E. Riedo, *Nat Mater*, 2012, **11**, 544-549.
17. S. Muhammad Hafiz, R. Ritikos, T. J. Whitcher, N. Md. Razib, D. C. S. Bien, N. Chanlek, H. Nakajima, T. Saisopa, P. Songsiriritthigul, N. M. Huang and S. A. Rahman, *Sensors and Actuators B: Chemical*, 2014, **193**, 692-700.
18. F. Yin, S. Wu, Y. Wang, L. Wu, P. Yuan and X. Wang, *Journal of Solid State Chemistry*, 2016, **237**, 57-63.
19. V. Țucureanu, A. Matei and A. M. Avram, *Critical Reviews in Analytical Chemistry*, 2016, **46**, 502-520.
20. J. R. Lomeda, C. D. Doyle, D. V. Kosynkin, W.-F. Hwang and J. M. Tour, *Journal of the American Chemical Society*, 2008, **130**, 16201-16206.
21. B. D. Ossoonon and D. Bélanger, *RSC Advances*, 2017, **7**, 27224-27234.
22. Z. Fan, K. Wang, T. Wei, J. Yan, L. Song and B. Shao, *Carbon*, 2010, **48**, 1686-1689.
23. L. Stobinski, B. Lesiak, A. Malolepszy, M. Mazurkiewicz, B. Mierzwa, J. Zemek, P. Jiricek and I. Bieloshapka, *Journal of Electron Spectroscopy and Related Phenomena*, 2014, **195**, 145-154.
24. K. Zhang, Y. Zhang and S. Wang, *Sci Rep*, 2013, **3**, 3448.
25. V. B. Mohan, R. Brown, K. Jayaraman and D. Bhattacharyya, *Materials Science and Engineering: B*, 2015, **193**, 49-60.
26. W. Chen, L. Yan and P. R. Bangal, *Carbon*, 2010, **48**, 1146-1152.